Ocean Dynamics (2017) 67:1495–1510
DOI 10.1007/s10236-017-1097-5

Floc size distributions of suspended kaolinite in an advection transport dominated tank: measurements and modeling

Xiaoteng Shen[1] · **Jerome P.-Y. Maa**[1]

Received: 1 December 2015 / Accepted: 25 August 2017 / Published online: 5 September 2017

Abstract In estuaries and coastal waters, floc size and its statistical distributions of cohesive sediments are of primary importance, due to their effects on the settling velocity and thus deposition rates of cohesive aggregates. The development of a robust flocculation model that includes the predictions of floc size distributions (FSDs), however, is still in a research stage. In this study, a one-dimensional longitudinal (1-DL) flocculation model along a streamtube is developed. This model is based on solving the population balance equation to find the FSDs by using the quadrature method of moments. To validate this model, a laboratory experiment is carried out to produce an advection transport-dominant environment in a cylindrical tank. The flow field is generated by a marine pump mounted at the bottom center, with its outlet facing upward. This setup generates an axially symmetric flow which is measured by an acoustic Doppler velocimeter (ADV). The measurement results provide the hydrodynamic input data required for this 1-DL model. The other measurement results, the FSDs, are acquired by using an automatic underwater camera system and the resulting images are analyzed to validate the predicted FSDs. This study shows that the FSDs as well as their representative sizes can be efficiently and reasonably simulated by this 1-DL model.

This article is part of the Topical Collection on the *13th International Conference on Cohesive Sediment Transport in Leuven, Belgium 7–11 September 2015*

Responsible Editor: Erik A Toorman

✉ Xiaoteng Shen
xiaoteng@vims.edu

[1] Virginia Institute of Marine Science, College of William & Mary, Gloucester Point, VA 23062, USA

Keywords Kaolinite · Flocculation · Floc size distributions · Streamtube model · Laboratory experiment

1 Introduction

Estuarine morphology is mainly influenced by mud deposition. Among all sedimentation processes, the settling of suspended particles is an important process to determine mud deposition (e.g., Chisholm 1999; McAnally 2000; Mietta 2010). Individual clay particles have little chance to settle on the bed because of their small sizes (< 2 μm), and thus, low settling velocities to resist upward transport. Clay sediments, however, are mostly present as flocs or aggregates as the result of flocculation that significantly alters their structure (i.e., size, density, and shape), which have higher settling velocities. In natural environments, flocs are formed after collision and attachment (because of cohesion) mainly due to the effect of turbulent shear, which practically limits the maximum floc size around the size of the Kolmogorov microscale. Nevertheless, because of the effect of bio-factors such as extracellular polymeric substances, it is not uncommon to find that the sizes of bio-aggregates are larger than the Kolmogorov microscale. Generally, aggregation decreases turbidity in the water body but increases siltation on the bed, while primary particles may increase turbidity and therefore attenuate light penetration in the water body. These environmental issues are largely related to the flocculation processes of suspended particles. Their floc size distributions (FSDs) are the most important indicator to quantitatively evaluate flocculation.

The flocculation process is not yet fully understood because it can be affected by many factors such as sediment concentration, clay mineralogy, local shear rate, floc strength, water chemistry (pH, salinity, and other ions), and organic

matter contents. Therefore, experiments that can isolate various affecting factors in order to understand the significance of each of the affected parameters in flocculation are important. These experiments also provide valuable data to validate any numerical model.

Three types of devices, Couette reactors, oscillating grids, and chamber/tank mixers (either using a paddle/propeller/impeller or a pump), have been commonly used to examine the FSDs of suspended particles (Serra et al. 2008). In Couette flow experiments (e.g., Zhu et al. 2015; Vlieghe et al. 2014; Wyatt et al. 2013; Bubakova et al. 2013; Yuan and Farnood 2010; Barbot et al. 2010; Frappier et al. 2010), the inner and outer cylinders can either both rotate (in the same or different directions), or only one rotates. The shear rate in this device for a laminar flow is constant and can be determined by the diameters and angular velocities of the cylinders. For a turbulent Couette flow, the shear rate also changes from outer cylinder to inner cylinder. Nevertheless, the gap between the inner and outer cylinders is limited, so that a floc will have a limited time to experience the change of shear rate. Serra et al. (2008) indicated that a Couette device produces larger flocs, compared with other flocculation devices that have the same average shear rate. This is because flocs in a Couette flow device are either under a constant shear rate everywhere, or flocs can only response to the average shear, and thus have time to develop.

Oscillating grids generate a reasonably homogenous turbulence field and are also widely used for studying flocculation processes and normally applied in settling columns/boxes (e.g., Pujol et al. 2010; Maggi et al. 2007). For small settling boxes, a micro-acoustic Doppler velocimeter (ADV) with a long "neck" can be inserted in the water column to measure turbulence directly (Pujol et al. 2010). Long settling columns can either provide zero-dimensional (0-D) conditions by only studying the floc conditions (e.g., size and density) at a selected location (Maggi et al. 2007) or provide one-dimensional (1-D) conditions by studying the floc conditions along the settling column (Van Leussen 1994). In the above two cases, a reasonable homogenous turbulence field is generated in the entire column by using oscillating grids. Rectangular grids are often used for a best turbulent shear production, and the average shear rates are controlled by the oscillation speed of the grids.

Mixing chamber experiments are the other types of setups used to study flocculation (e.g., Mietta et al. 2009; Kumar et al. 2010). For small tanks, turbulence is usually generated by a rotating impeller. Tank-averaged shear rate is determined by the impeller diameter, power number, rotational speed, and volume and viscosity of the fluid (e.g., Shen and Maa 2016a). By using the tank-averaged shear rate, it provides a 0-D case for studying flocculation. The FSDs at the measuring location are assumed to represent the tank-averaged FSDs because of short trajectories for flocs to travel within the tank. Therefore, the tank cannot be big in order to limit the length of trajectory. In cubic tanks, usually FSDs are determined from floc images taken through the transparent wall (Keyvani and Strom 2013, 2014; Shen and Maa 2016a), while another method is needed for cylindrical tanks since taking images through a curved wall may produce bias on FSDs. Note that even in these small mixing chambers, the flow field is not truly homogeneous. It is a complicated three-dimensional (3-D) flow that can be measured by using laser Doppler velocimeter (LDV; e.g., Ducoste et al. 1997) or particle image velocimetry technology (PIV; e.g., Ge et al. 2014). The spatial variability of FSDs within a small mixing chamber is limited because the time for a floc to travel among different shear zones is too short to reflect any significant change. Given enough time, the equilibrium FSD, which represents the balance of aggregation and breakup, can be assumed to display the results of the chamber-averaged shear rate (Ducoste et al. 1997).

In a relatively large tank (as used in this study, with a volume about 0.5 m^3), however, spatial variability of FSDs is measurable, although the differences are still limited. The shape of the tank is not important since the local FSDs are usually obtained by using an underwater camera system that takes pictures through a transparent cover of its waterproof house. The flow field can also be measured, e.g., by using an ADV device. The use of a laser in-situ scattering and transmissometer (LISST) instrument, however, is still difficult, because of its large size.

Besides laboratory experiments, numerical modeling is another tool to study flocculation processes. A flocculation model usually simulates the change of number density n for particles with size L at any location x and at any time t. For example, the population balance model (PBM) (e.g., Shen and Maa 2015) can be used to simulate the FSDs by solving N differential equations for $dn_i(L_i, x, t)/dt$ ($i = 1, 2, \ldots, N$) in which N is the number of size classes used to represent the FSD. PBMs have the advantage of considering various flocculation mechanisms (not limited to the effect of shear rate), and have the potential for further extension in order to couple with hydrodynamic models (e.g., Shao et al. 2017) or include more complicated floc properties (e.g., floc density) .

In this study, the FSDs of suspended kaolinite in an advection transport dominated tank are studied. It provides the chance to check the development of a 1-D longitudinal (1-DL) PBM that simulates the FSDs along an idealized streamtube. To achieve this objective, measurements of the flow field (e.g., mean velocity, turbulence kinetic energy, and energy dissipation rate) using an ADV-Ocean are carried out first. Those measured flow field results are used as inputs for the 1-DL model, which is an extension of a previously presented flocculation model for solving the FSDs (Shen and Maa 2015). Through an updated camera system, the measurements of FSDs are gathered to validate the modeling results.

2 Experimental setup and data analysis

2.1 Flow field measurements

Tap water in a cylindrical tank (diameter = 0.75 m; water depth = 1.1 m) was agitated by using a RULE 3700 GPH (gallon per hour) marine pump, mounted at the bottom of the tank (Fig. 1a). The pump outlet was modified by adding an adaptor, a 90° 1.5 in. PVC elbow, an 8 cm long 1.5 in. PVC pipe, and a 1.5 in. PVC diffuser cap with hand-drilled holes. The outlet was located at the center of the tank and 25 cm above the bottom of the tank. This setup generated an axially symmetric flow. The pump was powered with a fixed 12 V DC power supply for at least half an hour until the flow field reached a steady condition. Velocity and turbulence were measured by using a 5-MHz SonTek ADV-Ocean at selected points, and the measured values were used as inputs for the flocculation model.

The output of ADV-Ocean includes time series of instantaneous velocity components (incl. signal strengths and correlation parameters) for all three directions (SonTek 2001). At a few selected locations, where the signal strengths and correlations are high, data based on 10, 15, and 20 Hz measurement frequencies (with duration of 2, 4, and 6 min, respectively) are processed to check the differences of the mean velocities. Since there was found no significant difference, velocity measurements in this study are collected at 10 Hz for 2 min in these places, except for a few extremely high turbulence areas close to the pump outlet.

The raw velocity data were first filtered based on signal strength and its correlation. Signal strength is used to demonstrate if there are sufficient particles in the measuring site. For a good measurement, signal strength larger than 35 counts is required. This requirement is always satisfied in this study. The correlation coefficient evaluates the signal noise. In most places in the tank far from the pump outlet, the correlation is generally higher than 70%, with some places higher than 90%. For high turbulent flow near the pump outlet, however, a correlation as low as 30% is considered suitable in this study (SonTek 2001). Note that a sufficient amount of data (usually more than 70%) should be retained after filtering (Martin et al. 2002). For extremely high turbulence flow close to the pump outlet, little data may remain even after filtering with a 30% correlation. Increasing the velocity range is a practical way to increase the correlation coefficient (SonTek 2001). Although the basic principle for selecting a velocity range is to use the lowest range that can cover the maximum expected velocities, it is worth to increase the velocity range to reduce the noise and keep more data. If the problem of insufficient data would remain, these points may have to be excluded from the measurements (e.g., the points within 5 cm around the pump outlet in this study). After filtering the time series, the mean flow velocities are obtained by time averaging over 2 min.

Because of the axially symmetrical flow, the ADV-Ocean is held in such a manner that the direction of the marked sensor is aligned with the radial direction (r), measuring the radial velocity component, u. The other two sensors measure the vertical velocity component, w, in the direction, z, and the

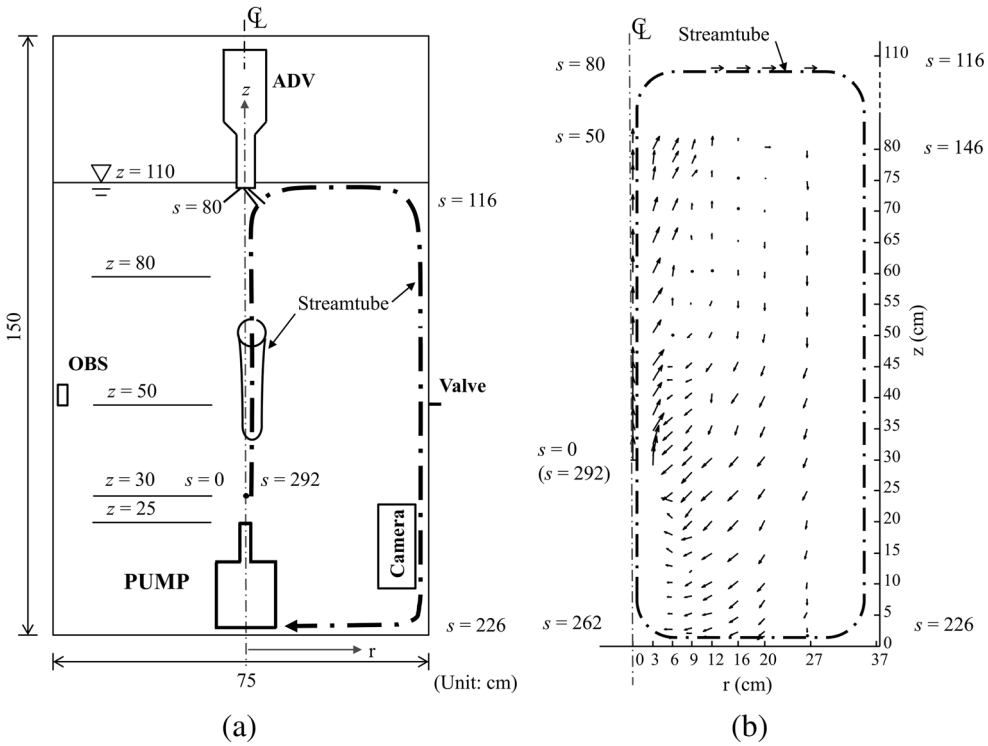

Fig. 1 Experimental setup. The drawing of the stream tube along the dashed line is not to scale. It is small near the pump and becomes large far away at the top due to jet spreading. It further increases at the horizontal section between s = 80 and 116 cm due to geometrical expansion. Along the side wall, between s = 116 and 226 cm, there is only minor change of the cross section due to the minor gain or loss of ambient water. The vertical coordinate, Z, starts at the tank bottom and the stream tube coordinate, s, starts at Z = 30 cm

tangential velocity component, v, in the θ direction. The flow field in the z-r plane in the tank is displayed in Fig. 1b. An idealized streamtube may be assigned which starts from a measurable point close to the outlet of the pump (s = 0), goes straight up until it is close to the water's surface at the center (s = 0 to 80 cm), and then turns 90° and goes horizontally to the side wall (s = 80 to 116 cm). From there, it turns another 90° and moves downward along the side wall from surface to bottom (s = 116 to 226 cm). Finally, it goes back to the pump and then returns to the starting point. Notice that the tangential velocity component is generally low, except at the bottom of the tank. The flow field below z = 80 cm is measured by holding the ADV downward as shown in Fig. 1a, while the flow close to the surface is measured by holding the ADV upside down. Therefore, the vertical velocity measured within s = 0 to 80, and 116 to 226 cm, is set as U_s (velocity along the streamtube), positive along the transport direction. For s = 80 to 116 cm, measured U velocity (which is parallel to the marked ADV receiver) is the main flow direction and thus it is set as U_s. The velocity at r = 36 cm (s = 116 to 226 cm) is assumed close to r = 27 cm, since it is the measured point closest to the side wall. Notice that U_s is always positive in this idealized streamtube.

The turbulent kinetic energy (TKE) is obtained as

$$K = \frac{1}{2}\left(\overline{\left(u'\right)^2} + \overline{\left(v'\right)^2} + \overline{\left(w'\right)^2}\right) \tag{1}$$

where u', v', and w' are velocity fluctuations with $u' = u - U$, $v' = v - V$, and $w' = w - W$, respectively, and the over bar denotes the time average within the time duration T. Note that de-spiking is required before calculating TKE. By trial-and-error, any fluctuation that is larger than five times of the standard variation is considered a spike and is discarded from the statistics.

In a turbulent flow, instability of the main flow produces an eddy with similar wave length or scale as the main flow. This eddy is unstable and disintegrates into smaller and smaller eddies until all of their energy is dissipated by viscosity and converted to thermal energy. To directly measure the energy dissipation rate, ε, is difficult, because it is hard to capture precisely the smallest turbulent structures (Saarenrinne and Piirto 2000). Tennekes and Lumley (1972) suggest that in the inertial subrange in the region of fully turbulent flow, the wave number-based energy spectral density E (m^3/s^2) can be expressed as

$$E(k) = A \cdot \varepsilon^{2/3} \cdot k^{-5/3} \tag{2}$$

where A is the 1-D Kolmogorov universal constant, ε is in units of square meter per cubic second, k (in units of m^{-1}) is the wave number, and the inverse of k is the size of the eddy. Since the ADV noise level is the lowest for the flow component parallel to the ADV source wave propagation direction, the vertical velocity spectrum is used in this study to estimate the energy dissipation rate (Feddersen 2010; Thomson et al. 2012; Nimmo Smith et al. 2005).

Results of Fourier transform of w (t) show energy at each frequency, f, thus it is necessary to transfer wave number k to wave frequency f. Based on the Taylor's frozen turbulence hypothesis, Lumley and Terray (1983) suggest

$$k = 2\pi / L = 2\pi f / W \tag{3}$$

in which L is the wave length, and W is the mean vertical velocity. Although Lien and D'Asaro (2006) suggest using instantaneous velocity instead of mean velocity, this study found that using instantaneous velocity merely introduces more spikes, and thus, was not used. Therefore, the energy spectrum based on wave frequency f can be obtained as (Fugate 2002; Thomson et al. 2012)

$$E(f) = A \cdot \varepsilon^{2/3} \cdot f^{-5/3} \cdot \left(\frac{W}{2\pi}\right)^{2/3} \tag{4}$$

The selected spectrum domain is from about 1 Hz (cf. Feddersen 2010) to about 5 Hz (Nyquist frequency, because of the 10 Hz sample frequency). As an example, Fig. 2 shows the non-smoothed velocity spectrum (in $m^2/s^2/Hz$). Because of the strong turbulence, it shows large scatter. Nevertheless, the inertial subrange is within this domain where the spectrum slope is − 5/3 (Fig. 2).

From Eq. 4, the energy dissipation rate ε can be estimated as (Fugate 2002; Liu et al. 2011; Thomson et al. 2012)

$$\varepsilon = \frac{2\pi}{W} \cdot \left(C / A\right)^{3/2} \tag{5}$$

where $C = E(f = 1)$ is the reading of energy at f = 1 Hz from the least square fitted line with a fixed slope of − 5/3 in the log-log plot of $E(f)$ vs. f. Although A is a constant on the order of 1, it is selected as 0.7 because of the suggestions that A = 0.71 from Liu et al. (2011) and A = 0.69 from Thomson et al. (2012). MATLAB codes for finding energy dissipation rate based on spectrum method can be found in Shen (2016).

Because the created flow field is quite complex, it is difficult to determine shear rates based on instantaneous velocity gradients. In this study, the turbulent shear rate G is defined as (e.g., Levich, 1962):

$$G = \sqrt{\frac{\varepsilon}{\nu}} \tag{6}$$

where ν is the kinematic viscosity of the fluid. The turbulent shear rate G is a Reynolds-averaged shear rate referring to the turbulent fluctuations only, following the actual definition of ε:

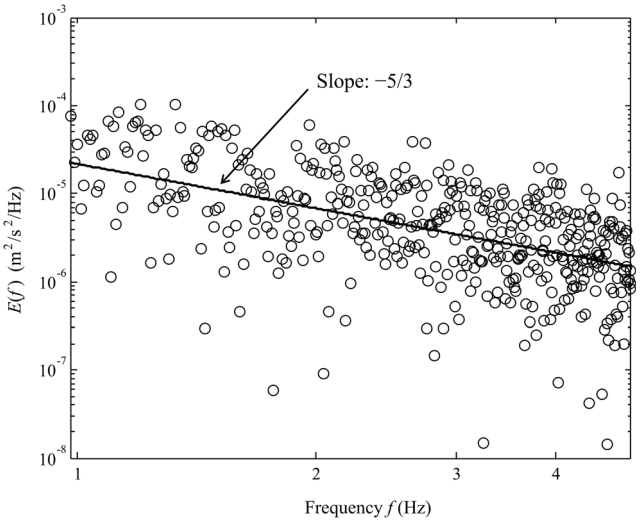

Fig. 2 Example of the energy dissipation rate calculated by using the vertical velocity component of the energy spectrum

$$\varepsilon = \nu \overline{\frac{\partial u'_i}{\partial x_j} \frac{\partial u'_i}{\partial x_j}} \tag{7}$$

Therefore, the definition of G simply follows from dimensional analysis and indeed is a measure of the averaged turbulent shear, which implicitly is assumed to be much larger than the averaged shear.

Kolmogorov (1941) proposes that the Kolmogorov micro length scale η_K, which is a length scale of eddy where viscosity is the major mechanism to dissipate energy (Thomas et al. 1999), can be estimated as

$$\eta_K = \left(\frac{\nu^3}{\varepsilon}\right)^{1/4} \tag{8}$$

This length scale can be used to determine the possible maximum floc size. The eddy diffusivity D is assumed close to the eddy viscosity and can be estimated by

$$D = C_\mu \frac{K^2}{\varepsilon} \tag{9}$$

in which $C_\mu = 0.09$ is a constant that is widely used in turbulence models (Rodi 1993).

2.2 FSD measurements

Initially kaolinite flocculated poorly since it was soaked in deionized water for more than 30 days to reach a fully water-saturated condition (Ha 2008). The pump made the flocs in the tank grow in a very short time and then break back to the original size in the pump. A properly selected amount of high concentration sediment-water mixture was poured into the cylindrical tank and diluted with tap water until the same water depth (i.e., z = 110 cm) was reached as that of the previous flow field measuring experiment. As shown in Fig. 1b, from s = 0 to s = 226 cm, the main flow is along the streamtube. The transport time from s = 0 to s = 226 cm is around 33 s, according to the measured mean velocities along the streamtube. It is difficult to estimate when the FSDs become locally steady, thus 48 h is waited to give sufficient time for the system to become stable. An optical backscatter sensor (OBS) is mounted at 50 cm above the bottom of the tank with the measuring point around 10 cm away from the wall. The measurements show the SSC is 0.38 g/L at the beginning and then slowly decreases to 0.36 g/L (Fig. 3). This result is based on the calibration results of SSC and OBS counts for the same kaolinite suspension carried out earlier in the mixing chamber experiments (Shen and Maa 2016a). Several water samples were also collected from the port on the tank's wall at t = 30 min, and the results also indicate that the average SSC is 0.4 g/L, which is close to the OBS monitoring results. If assuming the change of floc size distribution has no effect on the OBS calibration, an average SSC of 0.38 g/L may be used as one of the input parameters to model the FSDs along the entire streamtube.

An underwater camera system was developed to measure the FSDs of kaolinite suspensions. This camera system is based on that given by Shen and Maa (2016a) but improved for underwater uses. The technical details of this camera system can be found in Appendix A. The acquired floc images are processed using the MATLAB Image Processing toolbox, as reported by Shen and Maa (2016a) with some modifications. The procedures of image processing include converting RGB images (i.e., truecolor images) to grayscale images, removing background noise, contrast stretching and thresholding, removing small objects, dilation and erosion, filling the holes, removing on-border particles, and checking pixel gradients to remove out-of-focus flocs. Since the laser source is in green, only the green part of the RGB figure is extracted and its intensity is used to generate the grayscale image. The histogram of the grayscale image shows intensities varying from 10 to 180, with the span three times wider compared with that from the image taken with LED light source (Fig. 4). This is one of the advantages to using laser light, since a better quality image would span its light intensity on a wider range (full range is from 0 to 255). The background light intensity is estimated by finding the minimum light intensity for a pixel within a block of each 30 × 30 pixels. The resulting 163 × 108 square blocks are bi-interpolated to all pixels to generate a continuous background light intensity. Notice that the selected block in this study is much smaller than that used in an early version of the camera system (Shen and Maa 2016a). This is because the laser light is better than the LED light in this application for generating a finer grid background. The range of the intensity of the background is from 0 to 0.6 in this study, compared with 0.2 to 0.3 for

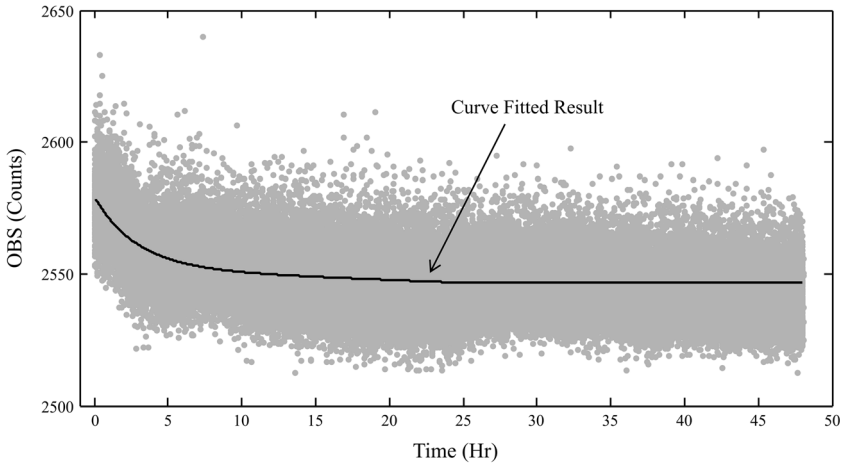

Fig. 3 Response of OBS counts during an experimental period

polystyrene particles used by Shen and Maa (2016a). Images are enhanced by a nonlinear contrast stretching with input intensity [0, 0.6] and mapping parameter 2 (mapping toward darker). Then, particles are separated and converted to a binary display using a constant threshold value 0.18 (a number determined by trial-and-error). Small objects with area less than 4 pixels or minor elliptic equivalent axis less than 2 pixels are removed as noise, dilation and erosion are applied to collect the morphology of flocs, and particles on the border are removed. The critical pixel gradient, which is estimated based on pixel gradient statistics, is set as 120. Any identified floc with a maximum pixel gradient below 120 is considered an out-of-focus particle or threshold noise, and thus, is removed. These values are used throughout this experiment. Circular equivalent diameter is thus calculated based on the number of pixels to construct a floc, and converted to floc size in microns based on the subject-to-image ratio (SIR) of the camera system.

3 Floc size distribution model

A simplified FSD model along a streamtube is presented. A bundle of nearby streamlines may be used to constitute a streamtube. For a steady turbulent flow, the location of the streamtube may be considered as a fixed tube in space. Since fluid only flows along the streamline, it assumes that the transport of sediment also mainly moves along the tube. As shown in Fig. 1a, this streamtube starts from $s = 0$ (close to the outlet of the pump where the velocity can be measured),

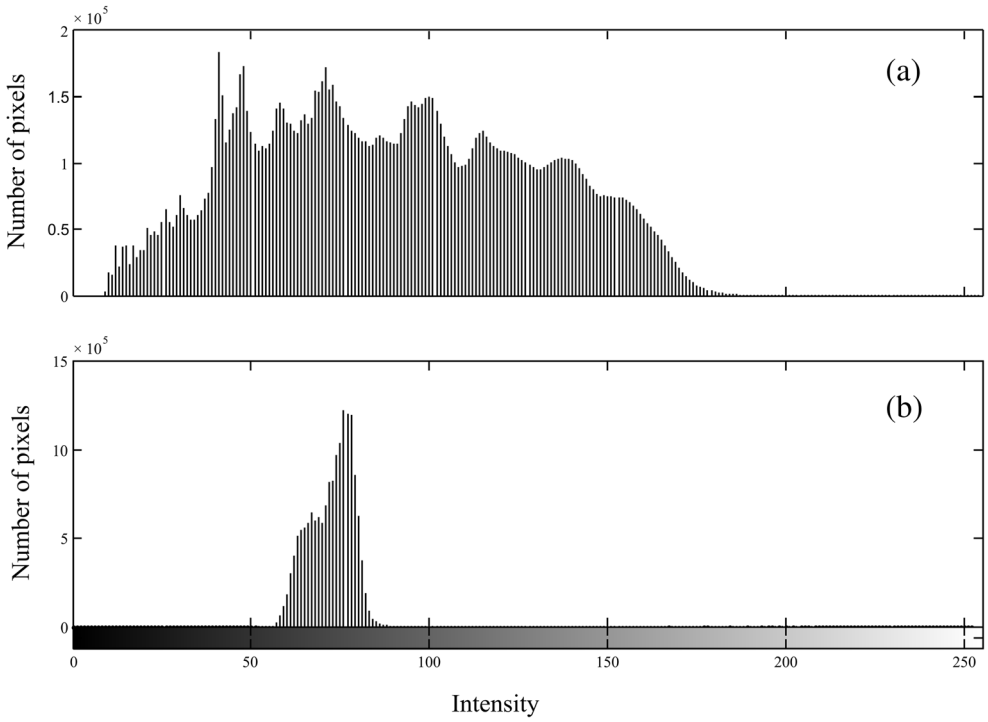

Fig. 4 Example of intensity diagram for the light source of **a** a green laser module and **b** 12 LEDs

goes along the measured streamline (with some degrees of idealization), and finally back to the pump and repeated again. The actual condition in our prediction is from $s = 0$ to $s = 226$ cm, and there is no measurement for $s > 262$ cm.

To find the governing equation for this 1-DL floc distribution model, consider a control volume along a streamtube between two control surfaces, CS 1 and CS 2 (Fig. 5), in which we focus on size L particles. These particles enter the control volume at CS 1 with a number density (number of particles with size L per unit volume) n. At this location, the streamtube cross section is A, and the mean velocity along the streamtube is U_s. When leaving the control volume at CS 2, the corresponding properties become $n + dn$, $A + dA$, and $U_s + dU_s$. Since $U_s >> w_s$ (settling velocity), settling is ignored in the formulation.

At time t, the control volume contains particles with various sizes. Among these sizes, particles of size L have number density n (L, s, t) at a location s and time t. At time $t + dt$, it is assumed that the floc remains in the streamtube, while the number density n (L, s, t) might alter. This is not only because particles enter or exit the control volume, but also because particles flocculate within the control volume. During the flocculation processes in the control volume, total particle mass is conserved but the particle number (either with all sizes and/or with a particular size L) may change because of aggregation and breakup processes. There may be turbulent exchange with the neighboring suspension, but here it assumes that its net contribution is negligible.

The governing equation for the change of total particle number (N) for a particular size L is based on a balance of local change, advective transport, and flocculation sources and sinks:

$$\frac{\partial}{\partial t}(N)_{Local} + (N_{out} - N_{in}) = \left(\dot{N}\right)_{Floc} \tag{10}$$

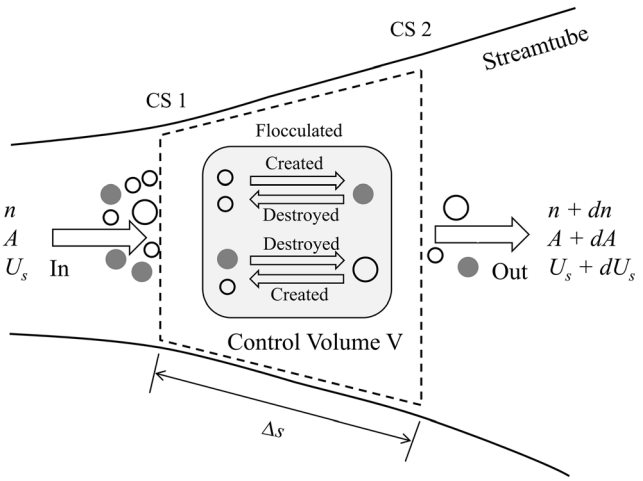

Fig. 5 Control volume to derive the governing equation of the 1-DL FSD model along a streamtube. Filled circles represent floc with size L and the number density of this size floc is n

in which N_{in} and N_{out} are the total particle numbers transported in and out of the control volume through the control surfaces CS1 and CS2, respectively, and $\dot{N}_{Floc}$ is the rate of particle number change due to flocculation processes within the control volume.

Since length of the control volume Δs and cross section A are selected as independent of time, the first term in Eq. 10 is given by

$$\frac{\partial}{\partial t}(N)_{Local} = \frac{\partial}{\partial t}(n{\cdot}A{\cdot}\Delta s) = A{\cdot}\Delta s{\cdot}\frac{\partial n}{\partial t}$$

The net difference of total number of size L particles entering and leaving the control volume (second term in Eq. 10) can be given as

$$\begin{aligned}
&= (n+\Delta n){\cdot}(U_s+\Delta U_s){\cdot}(A+\Delta A) - n{\cdot}U_s{\cdot}A \\
&\approx n{\cdot}U_s{\cdot}\Delta A + n{\cdot}A{\cdot}\Delta U_s + U_s{\cdot}A{\cdot}\Delta n \\
(N_{out}-N_{in}) &= n{\cdot}U_s{\cdot}\Delta s{\cdot}\frac{\partial A}{\partial s} + n{\cdot}A{\cdot}\Delta s{\cdot}\frac{\partial U_s}{\partial s} + U_s{\cdot}A{\cdot}\Delta s{\cdot}\frac{\partial n}{\partial s} \\
&= \left(n{\cdot}U_s{\cdot}\frac{\partial A}{\partial s} + A\frac{\partial (n{\cdot}U_s)}{\partial s}\right){\cdot}\Delta s
\end{aligned}$$

where higher order terms are ignored. The third term in Eq. 10 can be expressed as:

$$\left(\dot{N}\right)_{Floc} = S{\cdot}A{\cdot}\Delta s$$

Here, S represents the flocculation source and sink terms describing the rate of change of the number of size L particles per unit volume due to aggregation and breakup. As a consequence, the instantaneous number density n for a particular size L at time t in a steady flow field along a streamtube can be written as:

$$\frac{\partial n}{\partial t} + \frac{\partial (n{\cdot}U_s)}{\partial s} + \frac{n{\cdot}U_s}{A}{\cdot}\frac{\partial A}{\partial s} = S \tag{11}$$

Applying the classical Reynolds averaging procedure to decompose the instantaneous properties into time-averaged and fluctuant sections gives:

$$n = \overline{n} + n' \tag{12}$$

$$U_s = \overline{U_s} + U_s' \tag{13}$$

The cross section A is assumed to be independent of time, so that it does not have a turbulent contribution. The flocculation source and sink terms S is more or less empirical and therefore the turbulent contribution is neglected as well (Winterwerp and van Kesteren 2004). Substituting Eqs. 12 and 13 into Eq. 11 and averaging over the turbulent time scale gives

$$\frac{\partial \overline{n}}{\partial t}+\frac{\partial\left(\overline{n}\cdot\overline{U_s}\right)}{\partial s}+\frac{\partial\left(\overline{n'\cdot U_s'}\right)}{\partial s}+\frac{\overline{n}\cdot\overline{U_s}}{A}\cdot\frac{\partial A}{\partial s}+\frac{\overline{n'\cdot U_s'}}{A}\cdot\frac{\partial A}{\partial s}=S \quad (14)$$

Applying Fick's law, i.e., assuming the $\overline{n'\cdot U_s'}$ term is proportional to the gradient of time average number density along the streamtube, gives

$$\overline{n'\cdot U_s'}=-D\cdot\frac{\partial \overline{n}}{\partial s} \quad (15)$$

in which D is the turbulent diffusivity coefficient, which can be evaluated by assuming it is close to the eddy viscosity of the fluid.

Substituting Eq. 15 into Eq. 14 yields

$$\frac{\partial \overline{n}}{\partial t}+\frac{\partial\left(\overline{n}\cdot\overline{U_s}\right)}{\partial s}-\frac{\partial}{\partial s}\left(D\frac{\partial \overline{n}}{\partial s}\right)+\frac{\overline{n}\cdot\overline{U_s}}{A}\cdot\frac{\partial A}{\partial s}-\frac{D}{A}\cdot\frac{\partial \overline{n}}{\partial s}\cdot\frac{\partial A}{\partial s}=S \quad (16)$$

After this point the "bar" in $\overline{n}$ and $\overline{U_s}$ is omitted, thereby all variables are taken to be time-averaged. Therefore, the following governing equation for particles with a particular size L that specified its time-averaged number density n at time t in a steady flow field along a streamtube is obtained:

$$\begin{aligned}&\frac{\partial n(L,s,t)}{\partial t}+\frac{\partial(n(L,s,t)\cdot U_s(s))}{\partial s}-\frac{\partial}{\partial s}\left(D(s)\cdot\frac{\partial n(L,s,t)}{\partial s}\right)\\&+\frac{n(L,s,t)\cdot U_s(s)}{A(s)}\cdot\frac{\partial A(s)}{\partial s}-\frac{D(s)}{A(s)}\cdot\frac{\partial n(L,s,t)}{\partial s}\cdot\frac{\partial A(s)}{\partial s}=S\end{aligned} \quad (17)$$

In Eq. 17, the variables U_s, A, and D do not change with time, but do vary along the direction of the streamline s. The number density n is for a particular particle size L and can change with time t and space s. The flocculation source and sink term S can be expressed as (Shen and Maa 2015).

$$\begin{aligned}S=&\frac{L^2}{2}\int_0^L\left[\frac{\beta\left(\left(L^3-\lambda^3\right)^{1/3},\lambda\right)\cdot\alpha\left(\left(L^3-\lambda^3\right)^{1/3},\lambda\right)}{\left(L^3-\lambda^3\right)^{2/3}}\cdot n\left(\left(L^3-\lambda^3\right)^{1/3},s,t\right)\cdot n(\lambda,s,t)\right]d\lambda\\&-n(L,s,t)\int_0^\infty\beta(L,\lambda)\alpha(L,\lambda)n(\lambda,s,t)d\lambda+\int_L^\infty a(\lambda)\cdot b(L|\lambda)\cdot n(\lambda,s,t)d\lambda-a(L)\cdot n(L,s,t)\end{aligned} \quad (18)$$

in which λ is the integral variable with the same dimension of floc size L, $\beta(L, \lambda)$ is the Euclidean collision frequency function that describes the frequency of two spheres with size L and λ colliding to form a particle with size $(L^3 + \lambda^3)^{1/3}$, $\alpha(L, \lambda)$ is the collision efficiency that includes the effects of particle geometry, contact efficiency, and sticking probability, $a(L)$ is a breakup frequency function that denotes the frequency of disruption for particles with size L, and $b(L|\lambda)$ is a fragmentation distribution function that represents particles with size L produced by the breakup of a particle with size λ. The four terms in Eq. 18 include the following: the birth of flocs with size L due to aggregation of smaller particles, the death of flocs with size L due to aggregation with other particles, the birth of flocs with size L due to fragmentation of larger particles with size λ, and the death of flocs with size L due to themselves break up into smaller particles.

Equation 17 with flocculation source and sink terms represented by Eq. 18 is the governing equation for the number density of size L particles. To further track the number, surface area, volume, etc. of particles of all sizes, the quadrature method of moments is selected to solve the governing equation by applying Gaussian quadrature approximation with an adjustable factor, p. Details are given elsewhere (Shen and Maa 2015).

$$\begin{aligned}m_{k/p}(s,t)&=\int_0^\infty L^{k/p}n(L,s,t)dL\\&=\sum_{i=1}^{N_d}\omega_i(s,t)\cdot L_i(s,t)^{k/p}\left(k=0,1,\ldots,2N_d-1\right)\end{aligned} \quad (19)$$

in which n is integrated over the whole size range. $m_{k/p}$ is the (k/p)th order moments of FSD, with m_0 (i.e., $k = 0$), m_2 (i.e., $k = 2p$), and m_3 (i.e., $k = 3p$) proportional to the total number of all particles, total surface area, and total volume of all particles per unit fluid volume. The integral in Eq. 19 is numerically solved using N_d—node Gaussian quadrature approximation (Press et al. 1992) using N_d Gaussian quadrature nodes L_i ($i = 1, 2, \ldots, N_d$) and N_d corresponding weights ω_i ($i = 1, 2, \ldots, N_d$) by tracking the first $(2N_d - 1)$ moments $k = 0, 1, \ldots, 2N_d - 1$. The Gaussian quadrature nodes and corresponding weights are actually the characteristic sizes and number densities that can constitute the number-based FSD (Shen and Maa 2015). The variable p is an adjustable factor that controls the number of nodes (N_d) that can be tacked. For example, $p = 1, 2, 3, 4, 5$ for $N_d = 8$, and $p = 1, 2, 3, 4$ for $N_d = 7$. The optimum p is usually selected by trial-and-error.

Substituting Eq. 19 in Eqs. 17 and 18, the governing equation becomes

$$\frac{\partial m_{k/p}(s,t)}{\partial t}+\frac{\partial\left(m_{k/p}(s,t)\cdot U_s(s)\right)}{\partial s}-\frac{\partial}{\partial s}\left(D(s)\cdot\frac{\partial m_{k/p}(s,t)}{\partial s}\right)+\frac{m_{k/p}(s,t)\cdot U_s(s)}{A(s)}\cdot\frac{\partial A(s)}{\partial s}-\frac{D(s)}{A(s)}\cdot\frac{\partial m_{k/p}(s,t)}{\partial s}\cdot\frac{\partial A(s)}{\partial s}=S_{k/p}(L_i,\omega_i) \tag{20}$$

where

$$S_{k/p}(L_i,\omega_i)=\frac{1}{2}\sum_{i=1}^{N_d}\omega_i\sum_{j=1}^{N_d}\alpha(L_i,L_j)\cdot\beta(L_i,L_j)\cdot\omega_j\cdot\left(L_i^3+L_j^3\right)^{\frac{k}{3p}}+\frac{m_{k/p}(s,t)\cdot U_s(s)}{A(s)}\cdot\frac{\partial A(s)}{\partial s}-\frac{D(s)}{A(s)}\cdot\frac{\partial m_{k/p}(s,t)}{\partial s}\cdot\frac{\partial A(s)}{\partial s}=S_{k/p}(L_i,\omega_i)+\sum_{i=1}^{N_d}a_i\overline{b_i}^{(k/p)}\omega_i-\sum_{i=1}^{N_d}L_i^{k/p}a_i\omega_i \tag{21}$$

And

$$\overline{b_i}^{(k/p)}=\int_0^\infty L^{k/p}b(L|\lambda)dL \tag{22}$$

The flocculation kinetic kernels given in the above equation (i.e., collision frequency β, collision efficiency α, breakup frequency a, and fragmentation distribution function b) for suspended kaolinite can be summarized as (Smoluchowski 1917; Winterwerp 1999; Shen and Maa 2015)

$$\beta(L_i,L_j)=\frac{G}{6}\left(L_i+L_j\right)^3 \tag{23}$$

$$\alpha(L_i,L_j)=C_1 \tag{24}$$

$$a(L_i)=C_2\cdot\left(\frac{\mu}{F_y}\right)^{1/2}\cdot G^{3/2}\cdot L_i\cdot\left(\frac{L_i}{l_p}-1\right)^{3-nf} \tag{25}$$

$$\overline{b_i}^{(k/p)}=2^{(3-k/p)/3}L_i^{k/p} \tag{26}$$

in which G is the local shear rate, C_1 and C_2 are the aggregation and breakage parameters respectively, μ is the fluid dynamic viscosity, l_p = 5 μm is the representative primary particle size, F_y is the floc strength with a constant value of 10^{-10} N following the values given by Maggi et al. (2007) and Lee et al. (2011), and $nf = 3\cdot(L/l_p)^{-0.1}$ is the fractal dimension following the formulation given by Maggi et al. (2007) and Shen and Maa (2015) for suspended kaolinite. Equation 26 assumes a floc splits into two equal sized particles if it breaks up.

Note that Eq. 20 actually is a series of $(2N_d - 1)$ equations. At each time t, the left hand side of Eq. 20 is updated using a finite difference method, while the source and sink terms follow for Eq. 21 is a constant if the value of L_i (i = 1, 2, …, N_d) and ω_i (i = 1, 2, …, N_d) are available. A total of $2N_d$ variables of L_i and ω_i at time t are calculated from a finite set of $2N_d$ moments (m_0, $m_{1/p}$, …, $m_{(2Nd-1)/p}$) at time $(t-\Delta t)$ using Eq. 19 based on the long quotient modified difference algorithm (Sack and Donovan 1972; Wheeler 1974; Press et al. 1992; Shen and Maa 2015). Since advective transport dominates in this case, an explicit upwind scheme is used to avoid numerical instabilities. In this study, 14 moments with adjustable factor p = 4 were used to solve the seven size classes and seven corresponding number frequencies to construct the FSDs. The time step Δt is selected as 1.0×10^{-4} s for both transport and flocculation processes. Since the flow velocity is always positive along the streamtube, the upwind scheme actually becomes a backward difference scheme. The entire streamtube (292 cm) is divided into 58 grids with a resolution of 5 cm. The streamtube between s = 0 and s = 226 cm corresponds to cell numbers 1 to 45.

Note that the total mass of fluid and sediment (i.e., all particles) within the tube should be conserved, because the streamtube may be considered a rigid tube with no local storage (i.e., incompressible flow). This implies that the cross section areas of the streamtube are altered according to its mean velocity. The conservation of total sediment volume, i.e., m_3 (indicator of volume), remains unchanged, thus the source and sink term S_3 = 0 when $k = 3p$ in Eq. 20.

A repetitive boundary condition is applied for m_3 between the last and the first cell of the computational grid, i.e., m_3 in cell 59 is equal to m_3 in cell 1. This relation is also valid for the eddy diffusivity D, mean velocity u, and cross section A. For other moments $m_{k/p}$ ($k \neq 3p$), which are an indicator of FSD and other properties such as total particle number and total particle area, there is no need to specify the boundary condition because these moments at a downstream-most grid cell are only influenced by the one before.

4 Results and discussions

4.1 Model inputs

The presented 1-DL model is an extension of the previous 0-D model given by Shen and Maa (2015). Flow conditions and FSDs close to and away from the outlet of the pump should be different because of the significant different shear rates. This difference, however, cannot be identified by using a 0-D model. Near s = 0, the shear rate is extremely high, and particles may remain as primary particles. When close to the side wall, the shear rate is relatively low, and large flocs could be formed. Therefore, the presented 1-DL model was developed to elaborate such differences. Because of the limited traveling

time between the pump exit and near the tank wall, the difference of FSDs is not significant, but it shows some differences.

The measured flow properties along the streamtube are represented in Fig. 6, with $s = 0$ to $s = 80$ cm indicating a path near the center of the tank (center zone), $s = 80$ cm to $s = 116$ cm indicating close proximity to the water surface (surface zone), $s = 116$ cm to $s = 226$ cm indicating the side wall (side zone), and $s > 226$ cm indicating a return path for water to go back into the pump. Data from $s = 0$ to $s = 116$ cm are measured, while data from $s = 116$ to $s = 226$ cm at a radial distance $r = 37$ cm (Fig. 1b) are assumed close to the vertical component for the measured data at $r = 27$ cm. The velocities along the streamtube mainly change with the cross section of the streamtube. The minimum velocities around $s = 150$ cm and $s = 220$ cm (Fig. 6a) are due to the neighborhood of stagnation zones in the corners of the tank. Small size particles are expected in the high shear zone close to the outlet of the pump, while large flocs are expected far away. The turbulence close to the pump outlet is high, with the main flow $U_s > 80$ cm/s, the energy dissipation rate ε around 1000 cm^2/s^3, the TKE K around 1000 cm^2/s^2, and the eddy diffusivity D in the order of 100 cm^2/s. From $s = 0$ to $s = 80$ cm, U_s, ε, and K all decrease more than 1 order of magnitude, while D shows a local minimum at $s = 25$ cm. At the water surface from $s = 80$ cm to $s = 116$ cm, U_s and K show a gradual decrease, ε is relatively stable, and D continuously decreases to 1 cm^2/s. At the side from $s = 116$ cm to $s = 226$ cm, which is a vertical downward flow, U_s and K are relatively stable. D shows a parabolic character with small values at the surface and bottom of the side, while their local maximum is located around 30 cm above the bottom. ε continues to decrease until $s = 190$ cm, and it must increase again between 226 cm $< s <$ 262 cm, since the velocity increases along the tank bottom and toward the pump. The local shear rate G and Kolmogorov microscale η_K are proportional to 1/2 and − 1/4 power of ε, respectively, such that they display similar or reverse shape as that of ε. From Fig. 6e, it is clearly seen that the shear rate close to the pump outlet could be as high as 300 s^{-1}, while at $s = 190$ cm it may be as low as 5 s^{-1}. With this level of shear rate, the Kolmogorov microscale shows that the maximum floc size without organic matter influences usually cannot exceed 60–500 μm even with sufficient time for flocculation (Fig. 6f) (Mietta et al. 2009).

4.2 Model validation

The FSDs at $s = 130$, 145, 160, 175, 190, 205, and 220 cm are obtained by processing of the images taken by the underwater

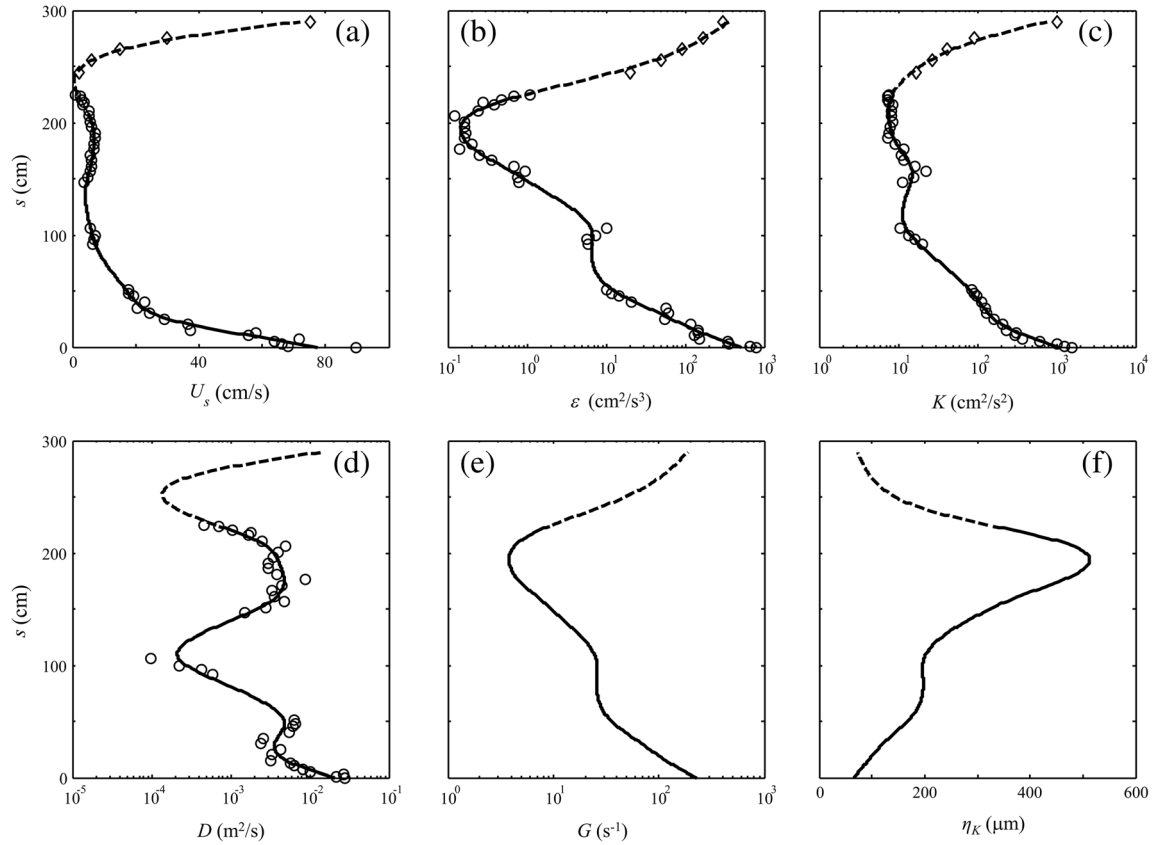

Fig. 6 Flow properties along the streamtube. Circles are measured results, and diamonds are estimated. Lines in **a**, **b**, and **c** are fitted results, while in **d**, **e**, and **f** are modeled results based on data shown in **b** and **c**. (U_s—flow velocity along the streamtube; ε—energy dissipation rate; K—TKE; D—eddy diffusivity; G—local shear rate; η_K—Kolmogorov scale)

camera system. Particles from a consecutive 50 images are used (more than 1000 particles) to have a stable FSD. In other words, all FSDs are the results of 2 min measurements that were displayed with a 5-μm bin size. These images were taken after running the pump for sufficient time to assure that locally steady conditions are obtained. All FSDs (Fig. 7) show a decreasing trend with its peak at the smallest bin. At s = 205 cm (about 20 cm above the bottom, close to the side wall), it has the most abundant small particles with a number fraction above 60%, while at other measuring points, the number fraction of flocs in the 5–10-μm bin varies around 40–50%. The short period for one cycle of a particle moving around along the streamtube is the reason why small particles are abundant because flocs do not have enough time to aggregate. It is important to notice that some flocs might travel out of the streamtube by turbulent dispersion, even though the measured velocity that represent cross-tube flow, from s = 0 to s = 226 cm, is low. Those flocs traveling outside of the streamtube may have the chance to become larger. Unfortunately, there is no data to investigate this assumption.

The original selected timing for taking images does not reflect the time for particles to achieve locally steady state, since it only takes 33 s for a particle to complete one circulation in the streamtube and, according modeling results, it takes 60 s to become steady (Fig. 8). Since this is an initial value problem (i.e., the FSD at any place along the streamtube is controlled by the strong pumping shear at the beginning), the 48-h waiting time (waiting for flocs arriving steady state) is not needed for this purpose. The waiting is to make sure that all sediments in the tank have passed through the pump and there is no long-term effect. In general, for an experiment where sediments have to go through high-and-low shear zones (e.g., a settling column with vibration screens, or a mixing chamber with a propeller), the waiting time is long (Maggi et al. 2007; Keyvani and Strom 2014). This long waiting, however, will not affect the fact that the flocculation process is completed in a short period of time. As discussed in Shen and Maa (2016b), the selection of absolute values for the parameters C_1 and C_2 should be based on matching the measured and predicted mean floc sizes at $t > 60$ s. Meanwhile, the ratio C_1/C_2 should be the same as that given in Shen and Maa (2016b)'s box model, which simulates the FSDs in a mixing chamber experiment using the same sediment. This is because the ratio C_1/C_2 determines the FSD at the final equilibrium state while their absolute values determine the growth pathway to arrive at the final state in the box model (Shen and Maa 2016b). The fitted C_1 and C_2 based on both flocculation path and final FSD in the 0-D modeling results can be used in a 1-DL model. By trial-and-error, $C_1 = 0.0325$ and $C_2 = 1.224 \times 10^{-6}$ are selected in this study for a reasonable match between the simulated and measured mean sizes at t = 60 s (Fig. 8). The ratio of C_1/C_2 is the same as that used in the Shen and Maa (2016b). It is important to note that the distance of measured data from s = 130 cm to s = 220 cm is relatively short, so the difference of their mean sizes are limited (especially when plotted on a logarithmic scale). The measured mean size at s = 205 cm is smaller than in other locations probably because of the turbulence is too low to promote flocculation, and without enough time, the particles cannot become large flocs. The model, however, does not reproduce this. This part may be improved by using a more complicated 3-D model in the future.

At t = 60 s, the normalized moments show the particle volume (m_3) along the tube is the same as that specified for the initial condition, which illustrates the conservation of total particle volume (mineral part) in the tube (Fig. 9). If the initial m_3 is not uniform along the tube, it will become uniform quickly because of strong advection transport. m_0, m_1, and m_2 show that the total particle number, total particle length, and total particle surface area continuously decrease from s = 0 to s = 150 cm while relatively unchanged in the side zone (Fig. 9). On the other hand, m_4 and m_5, which are proportional to the total

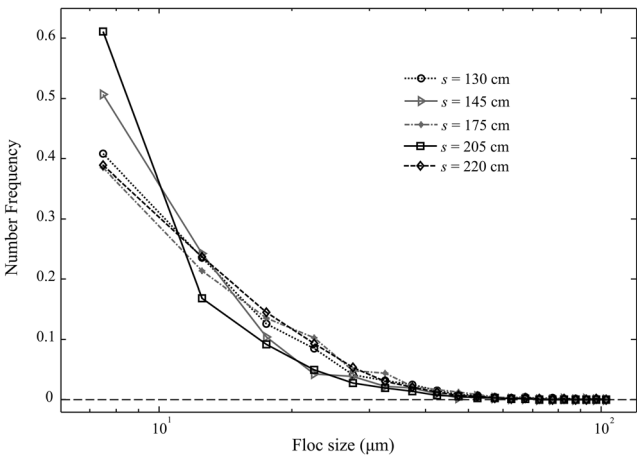

Fig. 7 Measured FSDs at varying elevation close to the side wall of the tank

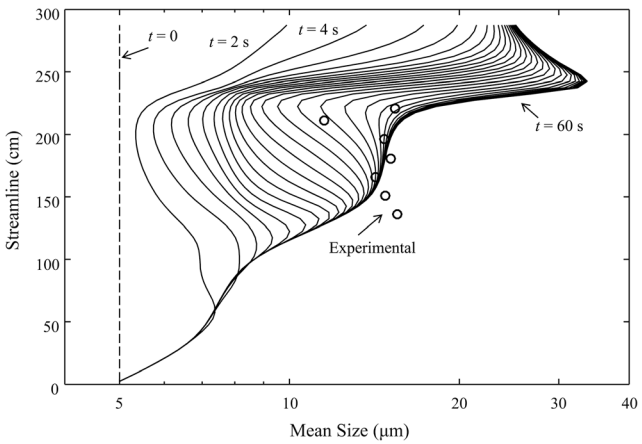

Fig. 8 Time evolution of mean size along the streamtube, with symbol "o" denoting measured results at t = 60 s

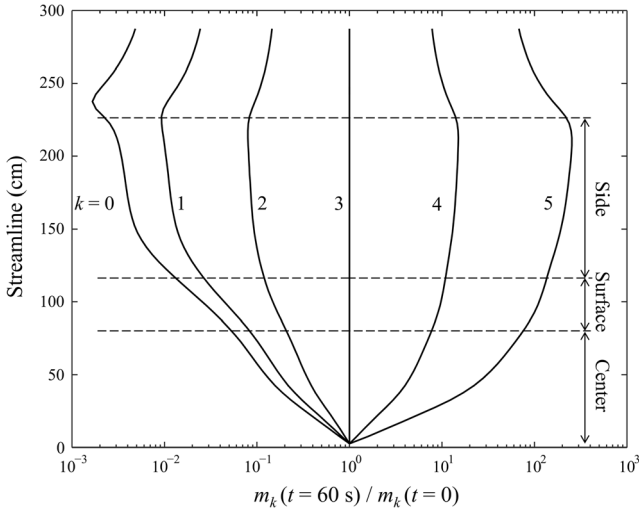

Fig. 9 Normalized moments m_k $(t)/m_k$ $(t = 0)$ $(k = 0, 1, 2, 3, 4, 5)$ at $t = 60$ s along the streamtube

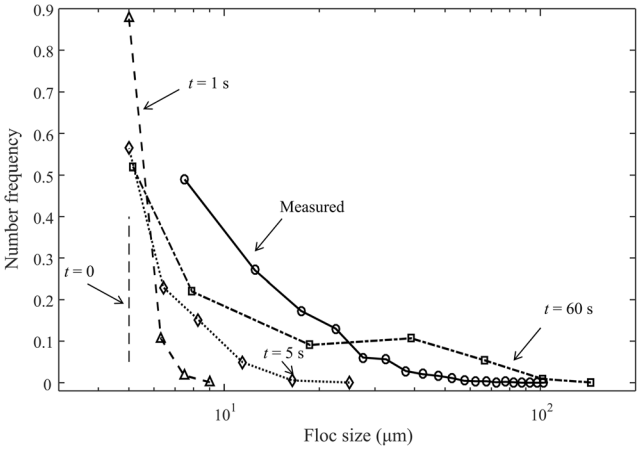

Fig. 11 Example of computed time evolution of FSDs at $s = 176$ cm in the side zone. Measured FSD at $t = 60$ s are also plotted for comparison

surface area of sediment settling per unit time and the settling flux (Mehta 2013), respectively, continuously increase (Fig. 9). The same m_3 at $s = 0$ (starting point) and $s = 292$ cm (ending point) also illustrate the assigned repetitive boundary condition of sediment volume in the tube. Other moments, however, do not have this boundary condition.

At the beginning of the simulation, the total number of all particles (m_0) is the same everywhere. Between $s = 0$ and 50 cm (center zone), this number changes quickly to an equilibrium, and does not change anymore because of strong shear. In the surface zone, m_0 approaches an equilibrium status with more time but less than the time of one circulation (Fig. 10). The side zone is the last place to approach the equilibrium status, and only this zone has reached the equilibrium status after $t = 60$ s.

At $t = 60$ s, the predicted FSDs at $s = 176$ cm are compared with measured results (Fig. 11). The error between the experimental and simulated FSDs is calculated using the following equation (Maggi et al. 2007)

$$Error = \frac{1}{2}\left(\sum_{i=1}^{N_d} |w_{Mi} - w_{Ei}|\right) \tag{27}$$

where $N_d = 7$, $\sum_{i=1}^{N_d} w_{Mi} = 1$, and $\sum_{i=1}^{N_d} w_{Ei} = 1$. w_{Mi} and w_{Ei} are modeled and experimental number frequencies for each size class, respectively. In this study, the error of the FSD at sizes 5, 8, 19, 39, 67, 102, and 145 μm (measured data are interpolated or extrapolate to these size classes) is 0.19. This error seems reasonable, as similar values (0.11–0.21) have been obtained in a settling column experiment by Maggi et al. (2007). The initial condition at $t = 0$, and simulated FSDs at $t = 1$ s, 5 s are also shown in this figure. It appears that the model prediction

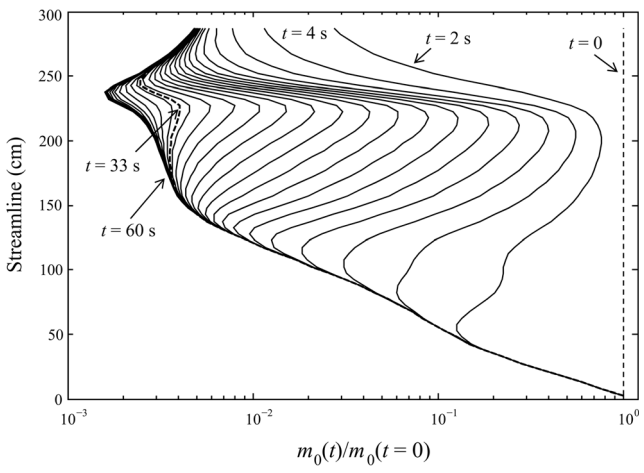

Fig. 10 Time evolution of total particle number along the streamtube. Lines are normalized and plotted every 2 s. The initial number is assumed the same along the streamtube

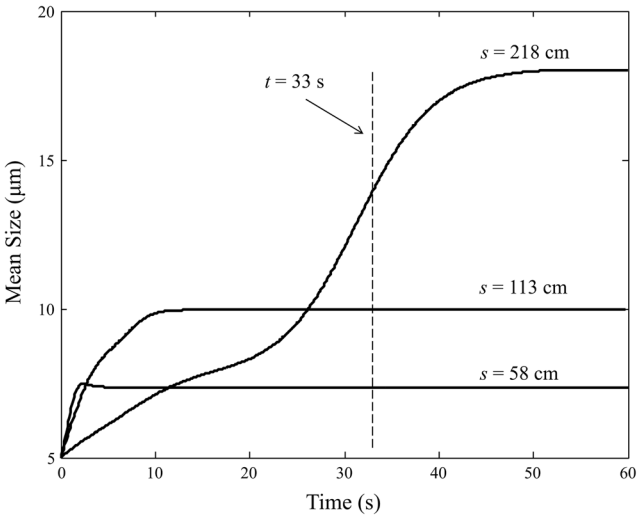

Fig. 12 Model predictions of time evolution of mean sizes at three selected locations

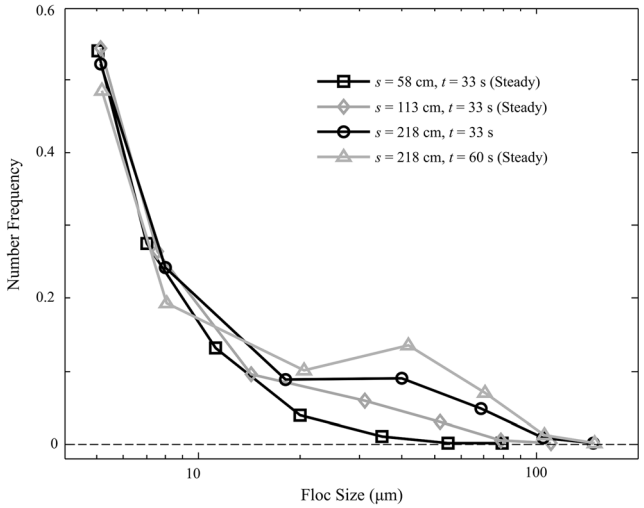

Fig. 13 Model predictions of FSDs at the equilibrium state for three selected locations

at t = 60 s has more large flocs. This is different from the measurements, and may be caused by a more favorable aggregation condition specified in the modeling. Besides, as examples of a few selected points, at s = 58 cm (at the center zone) and s = 113 cm (at the surface zone close to the starting point of the side zone), the time evolutions of the mean floc size show that it only takes 5 and 10 s to reach the equilibrium state (Fig. 12), with their predicted FSDs (Fig. 13) illustrating that most of the particles are small flocs, but some large flocs are also present. The flocculation process reaches steady state in such a short time because the flocculation time is inversely proportional to the shear rate (Colomer et al. 2005). Therefore, for the location at the outlet of the pump where the shear rate is extremely high, flocs must remain as primary particles. For the location far away from the pump, flocculation may require longer time to reach an equilibrium state. At s = 218 cm (close to the end of the side zone), however, the period for one cycle (t = 33 s) is less than that required to attain equilibrium (see Fig. 12), and thus, there are less large flocs compare with t = 60 s (Fig. 13).

5 Conclusions

A 1-DL flocculation model is developed to simulate the FSDs of suspended kaolinite in a streamtube whose boundaries are defined by streamlines. Water and sediment flow within the streamtube, with their velocity or sediment concentration distributions assumed uniform across the tube. The governing equations show the change of number density of a particular particle size based on a balance of local change, advection, diffusion, and flocculation. The settling term is omitted due to high advection in this case.

A laboratory experiment was carried out to validate this model. A 3700 GPH marine pump was placed at the bottom center of a 0.5-m^3 cylindrical tank, with its outlet re-fitted to eject fluid upward at the center to create an axially symmetrical flow. The flow field was measured by using a 5-MHz ADV-Ocean, and the measured data (mean flow, energy dissipation rate, turbulent kinetic energy, eddy viscosity, Kolmogorov micro length scale, and local shear rate) are put into the 1-DL model for solving the change of FSDs along the streamtube. Both the measured and predicted FSDs show a small particle dominated distribution, with the peak at the smallest particle size. The ratio of aggregation and breakage parameters C_1/C_2 is consistent with that obtained in a 5-L mixing chamber test for the same clay mineral (kaolinite). The absolute values of C_1 and C_2 depend on local environments, and they were determined by trial and error.

In this study, the flow condition is not the typical vertical 1-D flow, and not representative for natural environmental conditions. However, this 1-DL flocculation model can be easily extended to a 2-D longitudinal and vertical model to analyze cohesive sediment transport and flocculation in a conventional flume test. It can also be adapted for implementation into a 3-D sediment transport model, although the computational cost may be high for large-scale applications. This may provide a better method to study floc density and settling velocity of fine, cohesive sediments in the near future.

Acknowledgements The authors would like to thank two anonymous reviewers and the associated editor for their helpful comments for improving this manuscript. This paper is Contribution No. 3653 of the Virginia Institute of Marine Science, College of William & Mary.

Funding information This work and analysis was supported by the Virginia Institute of Marine Science (VIMS) Student Research Grant, a research grant (Contract number: 774080) from Korea Institute of Ocean Science and Technology (KIOST), China Scholarship Council (CSC) scholarship, the State Key Program of National Natural Science of China (Grant No. 41230640 & 51339005), and the National Natural Science Foundation of China (Grant No. 51409081).

Appendix A Details of the underwater camera system

This system was developed to measure the FSDs of kaolinite suspensions. This camera system is improved based on that given by Shen and Maa (2016a). It includes a Sony Alpha NEX-5R camera body with 4912 × 3264 pixels for images, a NEX E mount to Nikon F mount adaptor, three Kenko extension tubes (36 + 20 + 12 mm), a Nikon Macro Nikor 55 mm lens, and a +10 close-up lens that mounted sequentially (Fig. 14). These settings magnify the subject, from a subject size of 10.7 × 7.2 mm to an image size of 23.5 × 15.6 mm, i.e., a subject-to-image ratio (SIR) of 1: 2.2, and thus, changes the resolution from 4.8 μm per pixel to 2.2 μm per pixel. Using at least 2 × 2 pixels to identify a floc, the minimum sphere

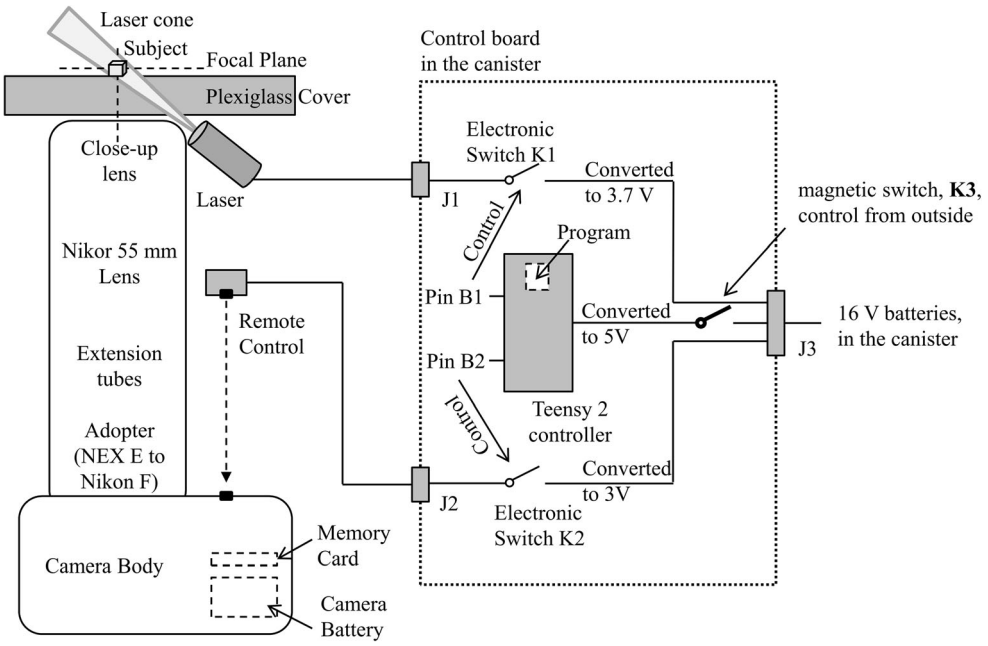

Fig. 14 Schematic diagram of the controlling system for acquiring images

equivalent floc size that can be identified by this camera system is around 5 μm, which is roughly consistent with the primary particle median size of cohesive sediment minerals in the natural environment. The shutter speed is set to 1/1000 s to catch the fast moving particles, the aperture is set at the maximum, f/2.8, to receive more lights and to limit the focus depth to about 2 mm. The ISO is set to 100 to minimize noise which may be considered as primary particles or small flocs. The trigger to take pictures is controlled by a commercially available remote control unit which is powered and controlled via a four-pin connector, J2, on the control board.

The major improvement on the current system is to replace the original LED light source by a 150 mW green laser module with a concave lens to spread the laser light. This laser module is mounted on the same side of the camera lens (i.e., front illumination) and points to the center of the image window. It is connected and controlled by the control board via a three-pin connector, J1. The above components are assembled and protected in a PVC tube with one cover made by PVC plate, and the other made by a 23-mm-thick plexiglass plate to allow pictures to be taken. Through air dielectric, the distance between the subject and lens (DSL) is slightly larger than 23 mm, but it increases to 29 mm when the plexiglass cover is placed between the lens and the subject. This gives around 5 mm distance between the cover and the front of the camera lens to take pictures for any subject that is within 1 mm of the other side of the plexiglass cover. The power for this camera system is provided by a set of four 18,650 lithium rechargeable batteries (i.e., 16VDC) inside the PVC tube via the connector, J3. This power is converted to 3.7 V to provide power for the laser source, converted to 5 V for the microcontroller, and converted to 3 V for the camera remote control. A magnetic switch which is attached on the PVC cover can be turned on if a magnetic bar is placed on the other side of the PVC cover. Once the switch is closed, the microcontroller begins to work following the instruction of the control program. This program generates periodic pulses which are fed into the gate of two field effect transistors (FETs), (i.e., 2N7000 and RFP2N08L, respectively) which behave as two electronic switches, K1 and K2. The timing of these two pulses match so that when the camera is taking images, the laser light is on. The program is set to take pictures every 2 s until the battery for the camera is exhausted. Nevertheless, this system operates for about 3 h before the batteries need to be changed. This working duration is sufficient for the current application, and much longer than the previous system (Shen and Maa 2016a) that uses LED light source. For field measurements in a typical tidal estuary, more improvements can be arranged to extend the operation duration. Finally, the acquired floc images are processed using the MATLAB Image Processing toolbox to statistically find the FSDs (Shen and Maa 2016a).

References

Barbot E, Dussouillez P, Bottero JY, Moulin P (2010) Coagulation of bentonite suspension by polyelectrolytes or ferric chloride: floc breakage and reformation. Chem Eng J 156(1):83–91. https://doi.org/10.1016/j.cej.2009.10.001

Bubakova P, Pivokonsky M, Pivokonsky R, Filip P (2013) The effect of shear rate on aggregate size distribution and structure at steady state: a comparison between a Taylor–Couette reactor and a mixing tank. J Water Supply Res T 62(5):288–295. https://doi.org/10.2166/aqua.2013.005

Chisholm TA (1999) A two-component aggregation model. Dissertation, Virginia Institute of Marine Science, College of William and Mary

Colomer J, Peters F, Marrase C (2005) Experimental analysis of coagulation of particles under low-shear flow. Water Res 39:2994–3000. https://doi.org/10.1016/j.watres.2005.04.076

Ducoste JJ, Clark MM, Weetman RJ (1997) Turbulence in flocculators: the effects of tank size and impeller type. AICHE J 43(2):328–338. https://doi.org/10.1002/aic.690430206

Feddersen F (2010) Quality controlling surf zone acoustic Doppler velocimeter observations to estimate the turbulent dissipation rate. J Atmos Ocean Tech 27(12):2039–2055. https://doi.org/10.1175/2010JTECHO783.1

Frappier G, Lartiges BS, Skali-Lami S (2010) Floc cohesive force in reversible aggregation: a Couette laminar flow investigation. Langmuir 26(13):10475–10488. https://doi.org/10.1021/la9046947

Fugate DC (2002) Estuarine suspended aggregate dynamics and characteristics. Dissertation, Virginia Institute of Marine Science, College of William and Mary

Ge CY, Wang JJ, Gu XP, Feng LF (2014) CFD simulation and PIV measurement of the flow field generated by modified pitched blade turbine impellers. Chem Eng Res Des 92(6):1027–1036. https://doi.org/10.1016/j.cherd.2013.08.024

Ha HK (2008) Acoustic measurements of cohesive sediment transport: suspension to consolidation. Dissertation, Virginia Institute of Marine Science, College of William and Mary

Keyvani A, Strom K (2013) A fully-automated image processing technique to improve measurement of suspended particles and flocs by removing out-of-focus objects. Comput Geosci 52:189–198. https://doi.org/10.1016/j.cageo.2012.08.018

Keyvani A, Strom K (2014) Influence of cycles of high and low turbulent shear on the growth rate and equilibrium size of mud flocs. Mar Geol 354:1–14. https://doi.org/10.1016/j.margeo.2014.04.010

Kolmogorov AN (1941) The local structure of turbulence in incompressible viscous fluid for very large Reynolds numbers. Proceedings of the USSR Academy of Sciences 30: 9−13. (in Russian, reprinted in 1991 in English. Proceedings of the Royal Society of London, Series A: Mathematical and Physical Sciences 434: 9–13)

Kumar RG, Strom KB, Keyvani A (2010) Floc properties and settling velocity of San Jacinto estuary mud under variable shear and salinity conditions. Cont Shelf Res 30(20):2067–2081. https://doi.org/10.1016/j.csr.2010.10.006

Lee BJ, Toorman E, Molz FJ, Wang J (2011) A two-class population balance equation yielding bimodal flocculation of marine or estuarine sediments. Water Res 45(5):2131–2145. https://doi.org/10.1016/j.watres.2010.12.028

Levich VG (1962) Physicochemical hydrodynamics. Prentice-Hall, Inc

Lien RC, D'Asaro EA (2006) Measurement of turbulent kinetic energy dissipation rate with a Lagrangian float. J Atmos Ocean Tech 23(7):964–976. https://doi.org/10.1175/JTECH1890.1

Liu H, Wu C, Ren J (2011) Estimation of turbulent kinetic energy dissipation rate in the bottom boundary layer of the Pearl River estuary. China Ocean Eng 25(4):669–678. https://doi.org/10.1007/s13344-011-0053-2

Lumley JL, Terray EA (1983) Kinematics of turbulence convected by a random wave field. J Phys Oceanogr 13(11):2000–2007. https://doi.org/10.1175/1520-0485(1983)013<2000:KOTCBA>2.0.CO;2

Maggi F, Mietta F, Winterwerp JC (2007) Effect of variable fractal dimension on the floc size distribution of suspended cohesive sediment. J Hydrol 343(1−2, 43):–55. https://doi.org/10.1016/j.jhydrol.2007.05.035

Martin V, Fisher TSR, Millar RG, Quick MC (2002) ADV data analysis for turbulent flows: low correlation problem. Hydraul Meas Exp Methods:1–10. https://doi.org/10.1061/40655(2002)101

McAnally WH (2000) Aggregation and deposition of estuarial fine sediment. Dissertation, University of Florida

Mehta AJ (2013) An introduction to hydraulics of fine sediment transport. World Scientific Publishing Company

Mietta F, Chassagne C, Winterwerp JC (2009) Shear-induced flocculation of a suspension of kaolinite as function of pH and salt concentration. J Colloid Interf Sci 336(1):134–141. https://doi.org/10.1016/j.jcis.2009.03.044

Mietta F (2010) Evolution of the floc size distribution of cohesive sediments. Dissertation, Delft University of Technology, Netherlands

Nimmo Smith WAM, Katz J, Osborn TR (2005) On the structure of turbulence in the bottom boundary layer of the coastal ocean. J Phys Oceanogr 35:72–93. https://doi.org/10.1175/JPO-2673.1

Press WH, Teukolsky SA, Vetterling WT, Flannery BP (1992) Numerical recipes in Fortran: the art of scientific computing, 2ed edn. Cambridge University Press, Cambridge

Pujol D, Colomer J, Serra T, Casamitjana X (2010) Effect of submerged aquatic vegetation on turbulence induced by an oscillating grid. Cont Shelf Res 30(9):1019–1029. https://doi.org/10.1016/j.csr.2010.02.014

Rodi W (1993) Turbulence models and their application in hydraulics. International Association for Hydraulic Research, 3rd edn. Balkema, Delft

Saarenrinne P, Piirto M (2000) Turbulent kinetic energy dissipation rate estimation from PIV velocity vector fields. Exp Fluids 29(1):S300–S307. https://doi.org/10.1007/s003480070032

Sack RA, Donovan AF (1972) An algorithm for Gaussian quadrature given modified moments. Numer Math 18(5):465–478. https://doi.org/10.1007/BF01406683

Serra T, Colomer J, Logan BE (2008) Efficiency of different shear devices on flocculation. Water Res 42(4−5):1113–1121. https://doi.org/10.1016/j.watres.2007.08.027

Shao Y, Shen X, Maa JPY, Shen J (2017) Simulating high ebb currents in the north passage of the Yangtze estuary using a vertical 1-D model. Estuar Coast Shelf S 196:399–410. https://doi.org/10.1016/j.ecss.2017.08.001

Shen X (2016) Modeling flocculation and deflocculation processes of cohesive sediments. Dissertation, Virginia Institute of Marine Science, College of William and Mary

Shen X, Maa JPY (2015) Modeling floc size distribution of suspended cohesive sediments using quadrature method of moments. Mar Geol 359:106–119. https://doi.org/10.1016/j.margeo.2014.11.014

Shen X, Maa JPY (2016a) A camera and image processing system for floc size distributions of suspended particles. Mar Geol 376:132–146. https://doi.org/10.1016/j.margeo.2016.03.009

Shen X, Maa JPY (2016b) Numerical simulations of particle size distributions: comparison with analytical solutions and kaolinite flocculation experiments. Mar Geol 379:84–89. https://doi.org/10.1016/j.margeo.2016.05.014

Smoluchowski M (1917) Versuch einer Mathematischen Theorie der Koagulationskinetik Kolloider Lösungen. Z Phys Chem 92:129–168 (in German)

SonTek (2001) ADV field acoustic Doppler velocimeter: technical documentation. SonTek/YSI Inc., California

Tennekes H, Lumley JL (1972) A first course in turbulence. Press, M.I.T

Thomas DN, Judd SJ, Fawcett N (1999) Flocculation modelling: a review. Water Res 33(7):1579–1592. https://doi.org/10.1016/S0043-1354(98)00392-3

Thomson J, Polagye B, Durgesh V, Richmond MC (2012) Measurements of turbulence at two tidal energy sites in Puget Sound, WA. IEEE J Ocean Eng 37(3):363–374. https://doi.org/10.1109/JOE.2012.2191656

Van Leussen W (1994) Estuarine macroflocs and their role in fine-grained sediment transport. Dissertation, University of Utrecht, Netherlands

Vlieghe M, Coufort-Saudejaud C, Frances C, Line A (2014) In situ characterization of floc morphology by image analysis in a turbulent Taylor–Couette reactor. AICHE J 60(7):2389–2403. https://doi.org/10.1002/aic.14431

Wheeler JC (1974) Modified moments and Gaussian quadratures. Rocky Mt J Math 4(2):287–296. https://doi.org/10.1216/RMJ-1974-4-2-287

Winterwerp JC (1999) On the dynamics of high-concentrated mud suspensions. Dissertation, Delft University of Technology, Netherlands

Winterwerp JC, van Kesteren WGM (2004) Introduction to the physics of cohesive sediment in the marine environment. In: van Loon T (ed) WL/Delft Hydraulics & Delft University of Technology, Delft, Netherlands

Wyatt NB, O'Hern TJ, Shelden B, Hughes LG, Mondy LA (2013) Size and structure of *Chlorella zofingiensis*/$FeCl_3$ flocs in a shear flow. Biotechnol Bioeng 110(12):3156–3163. https://doi.org/10.1002/bit.24996

Yuan Y, Farnood RR (2010) Strength and breakage of activated sludge flocs. Powder Technol 199(2):111–119. https://doi.org/10.1016/j.powtec.2009.11.021

Zhu Z, Yu J, Wang H, Dou J, Wang C (2015) Fractal dimension of cohesive sediment flocs at steady state under seven shear flow conditions. Water 7(8):4385–4408. https://doi.org/10.3390/w7084385